Photosynthesis   Hot Paper

The Electronic Origin of Far-Red-Light-Driven Oxygenic Photosynthesis

Abhishek Sirohiwal and Dimitrios A. Pantazis*

Abstract: Photosystem-II uses sunlight to trigger charge separation and catalyze water oxidation. Intrinsic properties of chlorophyll *a* pigments define a natural "red limit" of photosynthesis at ≈680 nm. Nevertheless, charge separation can be triggered with far-red photons up to 800 nm, without altering the nature of light-harvesting pigments. Here we identify the electronic origin of this remarkable phenomenon using quantum chemical and multiscale simulations on a native Photosystem-II model. We find that the reaction center is preorganized for charge separation in the far-red region by specific chlorophyll–pheophytin pairs, potentially bypassing the light-harvesting apparatus. Charge transfer can occur along two distinct pathways with one and the same pheophytin acceptor ($Pheo_{D1}$). The identity of the donor chlorophyll (Chl_{D1} or P_{D1}) is wavelength-dependent and conformational dynamics broaden the sampling of the far-red region by the two charge-transfer states. The two pathways rationalize spectroscopic observations and underpin designed extensions of the photosynthetically active radiation limit.

$\mathbf{P}$hotosystem-II (PSII) is a multi-subunit protein complex responsible for conversion of sunlight into chemical energy, driving oxidation of water into dioxygen.[1] Early events in the electron transfer cascade within PSII begin at the reaction center (RC, Figure 1)[2] composed of a central pair of chlorophylls P_{D1} and P_{D2}, accessory chlorophylls Chl_{D1} and Chl_{D2}, and pheophytins $Pheo_{D1}$ and $Pheo_{D2}$, arranged symmetrically along the D1 and D2 protein subunits.[3] Excitation energy transferred from antenna complexes to the RC initiates electron transfer along the D1 branch.[4] This creates a highly oxidizing radical cation that drives the catalytic cycle of water oxidation. Most oxygenic photosynthetic organisms employ Chlorophyll *a* (Chl *a*) and Pheophytin *a* (Pheo *a*) pigments in the RC, and Chl *a* pigments in light harvesting antennae. The longest wavelength captured by antenna chlorophylls that can efficiently drive PSII is ca. 680 nm, known as the "red limit" of oxygenic photosynthesis. Certain species of cyanobacteria[5] overcome this limit to thrive in low-light conditions by replacing selected Chl *a* pigments with far-red absorbing variants (Chl *d* and Chl *f*) in their antennae, and perhaps in the RC. However, this is not a precondition for far-red light utilization, because far-red light oxygenic photosynthesis has been confirmed in "normal" Chl *a* containing photosystems.[6] O_2 evolution using far-red photons is observed in nearly all photosynthetic organisms, including higher plants[6b] and green algae.[7] Charge separation in the PSII of these organisms can be induced at temperatures as low as 1.7 K.[8] Similar observations were made for Photosystem-I,[9] where charge separation can be triggered up to 840 nm, significantly longer than the "normal" threshold of 700 nm. The origin of this exceptional charge separation with far-red light in Chl *a* reaction centers is not understood. In this work, we identify the electronic origin of charge separation with far-red light using a multiscale approach based on a quantum mechanical/molecular mechanics (QM/MM) model of a complete PSII monomer and molecular dynamics (MD) simulations (Figures S1–S6), coupled with excited state computations using electrostatically embedded full time-dependent density functional theory with a range-separated functional. This was recently established as an optimal theoretical protocol for calculations of electrochromic shifts[10] and charge-transfer states[4c] of photosynthetic pigments through benchmarking against highly accurate equation of motion coupled cluster theory. The approach enables us to map the intrinsic light absorption profile of native PSII RC with unprecedented accuracy and develop a unified model for the presence of distinct, wavelength-dependent charge-separation pathways.

The protein matrix modulates site energies (lowest local excitation, Q_y band) of RC pigments in two ways, lateral and transverse,[4c] resulting in Chl_{D1} having the lowest site energy among all RC pigments (Table S1).[4c, 11] This is a feature of RC excitonic asymmetry, where protein electrostatics locate the sink of excitation energy on the active D1 branch. Analysis of vicinal pigment pairs additionally shows that the lowest excited state with excitonic character is localized on the Chl_{D1}–$Pheo_{D1}$ pair and that the nature of the excited state is a mixture of excitonic and charge-transfer (CT) $Chl_{D1}^+Pheo_{D1}^-$ character.[4c] The corresponding CT state involving the Chl_{D2}–$Pheo_{D2}$ pair on the inactive D2 is higher in energy, thus defining the excitonic-CT asymmetry of the RC, where the protein matrix stabilizes excited CT states on the D1 branch. Here we perform excited state calculations

[*] A. Sirohiwal, D. A. Pantazis
Max-Planck-Institut für Kohlenforschung
Kaiser-Wilhelm-Platz 1, 45470 Mülheim an der Ruhr (Germany)
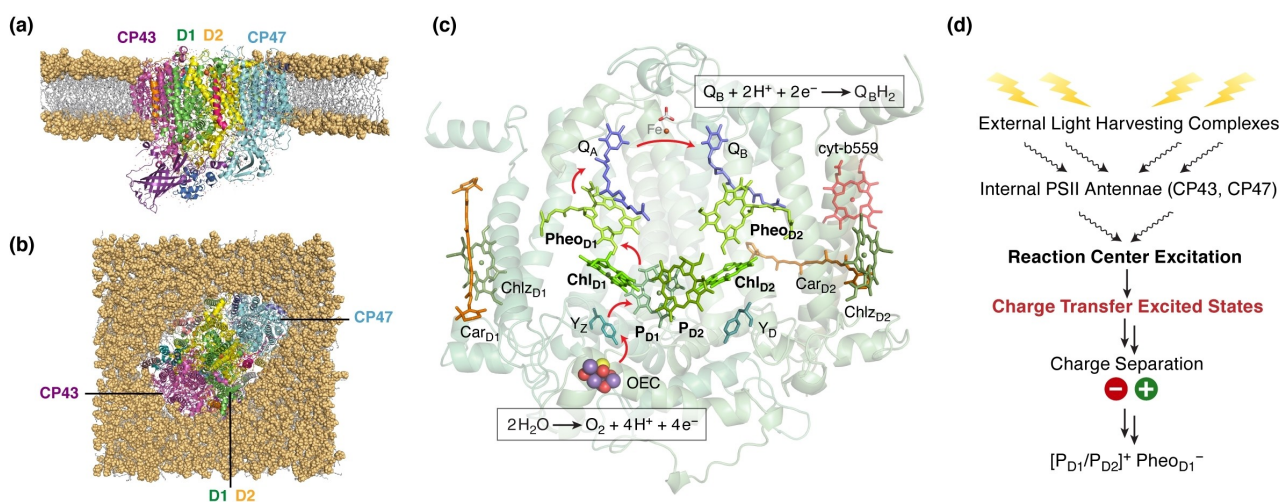E-mail: dimitrios.pantazis@kofo.mpg.de

Figure 1. a) Side view and b) top view of the molecular-mechanics model of the lipid bilayer bound PSII monomer used in molecular dynamics simulations. Proximal antenna complexes (CP43 and CP47) and core reaction center proteins (D1 and D2) are indicated. c) PSII catalyzes the four-electron water oxidation at the oxygen-evolving complex (OEC) and the two-electron plastoquinone (Q_B) reduction. The red arrows indicate the flow of electrons from the donor to the acceptor terminals of PSII along the active D1 branch of the enzyme. d) Light harvesting by external chlorophyll–protein complexes is followed by excitation energy transfer in a "funneling" manner to the CP antenna complexes and finally to the reaction center. Excited states with charge-transfer character resolve to charge-separated states, eventually localizing the positive charge on the central $P_{D1}P_{D2}$ pair of chlorophylls. This linear scheme does not explain the ability of far-red light to initiate charge separation.

with electrostatically embedded quantum mechanical regions comprising contiguous pigment tetramers, which allows us to capture the complete excitonic and CT energy landscape of the RC. A total of 22 uncorrelated structural configurations of the protein were studied, derived from a 200 nanoseconds molecular dynamics simulation. Snapshot 1 corresponds to a "crystal structure configuration" of PSII,[3d] derived from the early equilibrated structure, whereas other snapshots are derived from unbiased production MD simulations with 10 nanoseconds intervals.

In all snapshots the low-energy spectrum contains excited electronic states with significant charge-transfer character (detailed results provided in Tables S2–S26). Two classes of low-lying states are identified for the active-branch P_{D1}-P_{D2}-Chl_{D1}-$Pheo_{D1}$ pigment assembly: a) charge-transfer states of $Chl_{D1}^+Pheo_{D1}^-$ and $P_{D1}^+Pheo_{D1}^-$ character, and b) locally excited (LE) states on Chl_{D1} and P_{D1}/P_{D2}. The LE Chl_{D1} and CT $Chl_{D1}^+Pheo_{D1}^-$ character is almost always mixed and appears in more than one low-lying states. Protein dynamics affect the CT and local excitations differently. The energetics of CT states are highly dependent on conformational changes, therefore a wide energy range is observed due to their large dipole moment and strong coupling with the protein electrostatic field. The lowest local excitation is most often on Chl_{D1}, typically mixed with minor $Chl_{D1}^+Pheo_{D1}^-$ CT character. Local excitations are not significantly affected by protein dynamics, thus the energy range associated with the Chl_{D1} LE state spans 1.772–1.839 eV, i.e. in the red region around 680 nm (energy variation of 0.067 eV or 540 cm^{-1}).

The $Chl_{D1}^+Pheo_{D1}^-$ CT character is always present in either the first or second excited state (S_1 or S_2) of all 22 snapshots. It shows an energy variation of 1.474–1.893 eV (span of 0.419 eV or 3379 cm^{-1}), thus sampling the red and

far-red region in all snapshots. The mixing of LE and CT character confers significant oscillator strength compared to the $P_{D1}^+Pheo_{D1}^-$ CT state, therefore the $Chl_{D1}^+Pheo_{D1}^-$ state can be directly photoexcited by far-red light. The P_{D1}^+ $Pheo_{D1}^-$ CT state has negligible oscillator strength (dark state) due to diminishing spatial overlap between donor and acceptor orbitals, and is considerably more sensitive to conformational dynamics, spanning a wider energy range of 1.380–2.305 eV (variation of 0.925 eV or 7461 cm^{-1}). The ordering of these two CT states can switch depending on conformational dynamics. Thus, although a state of Chl_{D1}^+ $Pheo_{D1}^-$ CT character is always found within the two lowest excited states, the $P_{D1}^+Pheo_{D1}^-$ CT state is the lowest excited state (S_1) in six of the 22 snapshots and energetically comparable to $Chl_{D1}^+Pheo_{D1}^-$ states in almost half of them, but its sensitivity to conformational dynamics also pushes it to energies of ca. 2 eV or more in 10 of the 22 snapshots. The wide span of the $P_{D1}^+Pheo_{D1}^-$ CT state however means that it can also reach further into the far-red than states of $Chl_{D1}^+Pheo_{D1}^-$ CT character.

The natural transition orbitals (NTOs) depicted in Figure 2 provide a concise description of the electronic nature of three excitations that dominate the low-energy spectrum of the PSII RC (see also Figures S6–S9). Crucially, CT states involving the "special-pair" ($P_{D1}P_{D2}$), such as $P_{D1}^+P_{D2}^-$ and $P_{D1}^+Chl_{D1}^-$ (Figures S10 and S11) are found consistently above 3 eV. This confirms that physiological primary charge separation in PSII does not occur within the central pair of chlorophylls, while the $P_{D1}^+Chl_{D1}^-$ state is also excluded as an intermediate state in charge separation.[4c, 12] The above results describe exactly two possible low-energy CT states in the active branch of the PSII RC, both of them involving $Pheo_{D1}$ as the site of negative charge, while protein conformational motion enables enhanced sampling of the
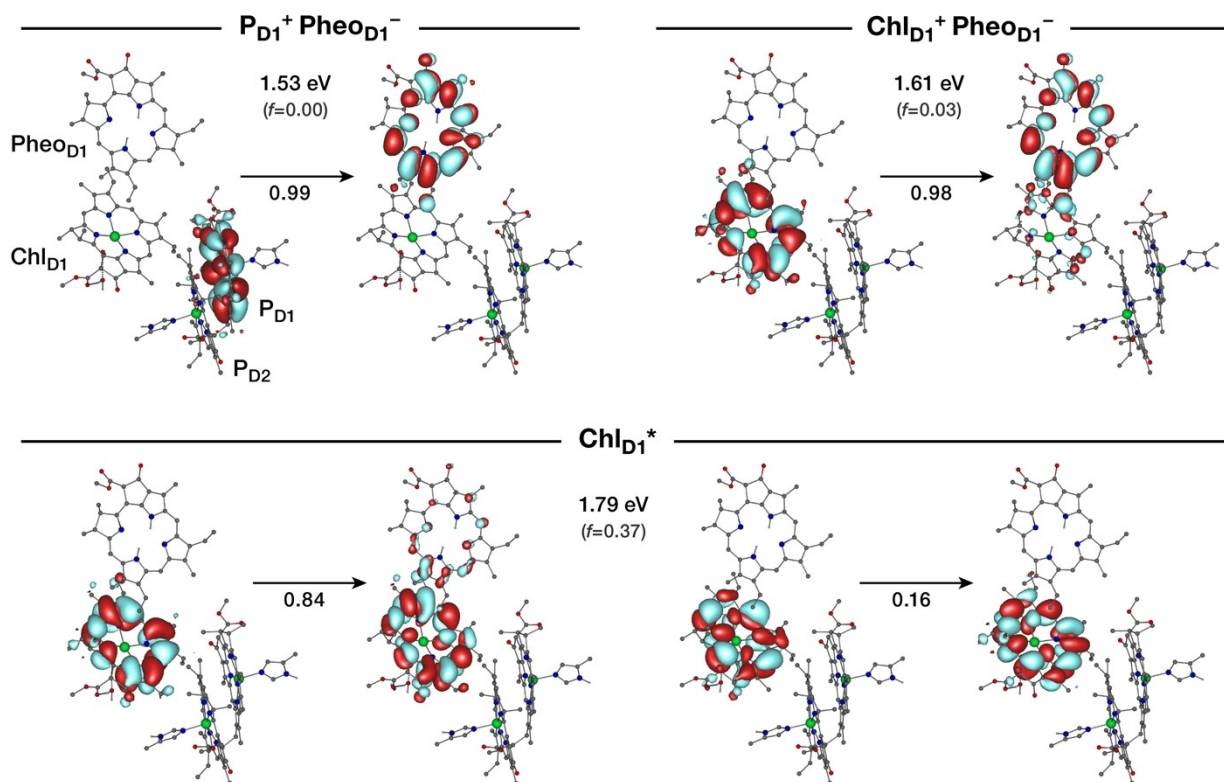
Figure 2. Donor/acceptor pairs of natural transition orbitals (NTOs) describing specific low-energy excited states of the P_{D1}-P_{D2}-Chl_{D1}-$Pheo_{D1}$ active branch tetramer. The orbitals shown were obtained from snapshot 1, to which the energies, oscillator strengths, and NTO coefficients correspond. The S_1 and S_2 states in this snapshot have $P_{D1}^{+}Pheo_{D1}^{-}$ and $Chl_{D1}^{+}Pheo_{D1}^{-}$ character, while the S_3 state is a local Chl_{D1} excitation. The properties and NTO characterization of low-lying states for all snapshots are tabulated in the Supporting Information. Charge transfer states of $P_{D1}^{+}P_{D2}^{-}$ or $P_{D1}^{+}Chl_{D1}^{-}$ character are found at much higher energies.

far-red region by these two excited states, albeit to different extent.

The protein matrix is essential for maintaining the asymmetry within the RC and creating the low-lying CT states in the far-red region. This is because chlorophylls and pheophytins experience negative and positive electrostatic potential, respectively.[4c] This reverse polarization effect of the protein matrix explains the enhanced stabilization of $P_{D1}^{+}Pheo_{D1}^{-}$ and $Chl_{D1}^{+}Pheo_{D1}^{-}$ excited CT states and destabilization of $P_{D1}^{+}Chl_{D1}^{-}$ and $P_{D1}^{+}P_{D2}^{-}$ CT states. Calculations performed in the absence of the electrostatic field of the protein matrix result in absence of CT states from the low-energy spectrum (Table S2), which is dominated by pure local excitations. This reaffirms that RC function is conferred by protein matrix electrostatics[4c, 11] and is not intrinsic to pigment arrangement or conformation.

Experimental detection of CT states in the far-red region using linear absorption spectroscopy is difficult due to the low oscillator strength. This is obvious for the $P_{D1}^{+}Pheo_{D1}^{-}$ state. Nevertheless, absorption spectroscopy studies under cryogenic conditions (1.7 K) by Krausz and co-workers[8a] on highly concentrated PSII samples were able to locate absorption features in the 700–730 nm range. Compared to our results, this feature could originate from the Chl_{D1}^{+} $Pheo_{D1}^{-}$ CT state, which has mixed excitonic character leading to slightly higher oscillator strength.

The present results clarify the electronic nature of CT pathways that can operate in PSII. The lowest excited state with local excitonic character is formed at Chl_{D1}, therefore this can function as the sink of excitation energy arriving from antenna complexes. Mixing of excitonic and CT character aids in smooth exciton dissociation to form the $Chl_{D1}^{+}Pheo_{D1}^{-}$ state as the primary charge-separated state. Subsequently, electron transfer from P_{D1} to Chl_{D1} can create the $P_{D1}^{+}Pheo_{D1}^{-}$ charge-separated state. Therefore, Chl_{D1} and $Pheo_{D1}$ act as the primary electron donor and acceptor, respectively, under "red-limit" photosynthesis. The situation under far-red light is more intriguing, because both P_{D1}^{+} $Pheo_{D1}^{-}$ and $Chl_{D1}^{+}Pheo_{D1}^{-}$ CT states can reach into the far-red thanks to their sensitivity to protein conformational dynamics. Depending on wavelength, the two CT states can be excited (directly or indirectly) resulting in both Chl_{D1} and P_{D1} being able to act as primary electron donors. Irrespective of which far-red CT pathway is productive, the primary electron acceptor would always be $Pheo_{D1}$,[13] while the created electron hole would eventually be stabilized on P_{D1} or distributed among P_{D1}/P_{D2}.[14] Our results therefore support the existence of parallel charge-separation pathways in PSII,[15] but with differences from analogous ideas discussed previously. Specifically, Chl_{D1} is the primary donor

Angew. Chem. Int. Ed. **2022**, 61, e202200356 (3 of 5)

© 2022 The Authors. Angewandte Chemie International Edition published by Wiley-VCH GmbH

activated either via EET or directly by red and far-red light, whereas P_{D1} may be activated in the far-red regime. Importantly, the charge-separation pathways are dependent on both protein conformation and excitation wavelength.

As discussed in the Supporting Information, direct access to a low-lying $P_{D1}^+Pheo_{D1}^-$ CT state may be one feature that distinguishes PSII from Type-I photosystems and the bacterial reaction center (BRC). The number of accessible CT states in the low-energy spectrum and the localization of the sink of excitation energy on Chl_{D1} leads to divergence of the charge-separation picture between these systems.

A key question concerns the effectiveness of far-red light driven charge separation. Experiments on intact spinach PSII samples showed full charge separation in the RC using far-red light at 5 K[8b] based on the EPR signal of secondary electron donor species (such as the Y_Z, Car_{D2}, Chl_Z and Cyt_{b559}). It was found that 730 nm, 740 nm and 750 nm wavelengths induced charge separation in 42%, 37% and 11% of PSII. This key result means that a) charge separation solely due to far-red light is more effective in the wavelength range of 700–740 nm, and b) the energy range populated by the low-lying $Chl_{D1}^+Pheo_{D1}^-$ and $P_{D1}^+Pheo_{D1}^-$ states is relatively wide. According to the present study, 700–740 nm would mostly excite the $Chl_{D1}^+Pheo_{D1}^-$ CT state owing to its higher oscillator strength, as the far-red limit of charge-separation in PSII is close to 800 nm. This can be correlated with the yield of the secondary electron donor species, because higher yield of $Y_Z/CaMn_4$ oxidation was observed compared to the yield of $Cyt_{b559}/Chl_Z/Car_{D2}$ using 730 nm, 740 nm and 750 nm wavelengths. It is likely that the electron hole after charge separation resides on Chl_{D1} under cryogenic conditions since electron donation from P_{D1} would require further structural reorganization that is probably inhibited. Therefore, electron donation from Y_Z is preferred based on distance. A small but significant yield of $Cyt_{b559}/Chl_Z/Car_{D2}$ is also observed; our results suggest this is possible under two conditions: a) when the P_{D1} pathway is activated in some PSII centers, and b) in PSII centers that contain nearly isoenergetic $Chl_{D1}^+Pheo_{D1}^-$ and $P_{D1}^+Pheo_{D1}^-$ CT states, owing to which $Chl_{D1} \rightarrow P_{D1}$ hole migration may be feasible even at cryogenic temperatures. Similar conclusions regarding primary charge separation pathways were drawn based on oxidation kinetics of the Y_Z and Y_D radicals with 732 nm light.[16]

Far-red light alone can drive oxygen evolution, albeit with reduced yield.[6a,17] The present results suggest this is due to the high dependence of the energetics of $Chl_{D1}^+Pheo_{D1}^-$ and $P_{D1}^+Pheo_{D1}^-$ CT states on conformational dynamics. Few PSII centers would complete charge-separation with far-red light and since four successive charge separations are required for successful evolution of O_2, there is reduced probability that a far-red light driven process will regularly outcompete charge recombination to complete the catalytic cycle of water oxidation. The above explain experimental observations on O_2 evolution in the far-red light range (700–800 nm), where a significant dip in PSII quantum yield above 680 nm was observed, but with an intriguing local maximum at ≈745 nm.[6a,17] In light of the present results the unexpected increase in O_2 yield may be

attributed to this wavelength range being populated by both far-red CT states, increasing the probability of charge separation.

In conclusion, we demonstrated that the low-energy excited states of the PSII RC consist of two types of charge-transfer states, with either $Chl_{D1}^+Pheo_{D1}^-$ or $P_{D1}^+Pheo_{D1}^-$ character. Far-red light is able to trigger charge separation within the reaction center of PSII through direct or indirect excitation of these two types of accessible CT states. Which charge separation pathway will be mostly activated depends on conformational dynamics, the wavelength of incident light, and intensity transfer mechanisms. Recent studies support the importance of far-red light in enhancing photosynthetic efficiency.[18] Both red and far-red light driven charge-separation likely work in conjugation to advance photosynthetic activity, which can be critically important for photosynthetic organisms living in shaded environments such as forest canopies, and when EET to the RC becomes rate-limiting.[19] In such cases far-red photons can induce charge separation by directly exciting CT states of the RC, moving the photochemistry forward. The present results provide an electronic structure rationalization for such observations. They also offer potential gateways toward protein-based rather than pigment-based extensions of photosynthetically active radiation beyond the red limit, i.e. via modification of protein matrix electrostatics rather than chemical modification of pigments.

Conflict of Interest

The authors declare no conflict of interest.

Data Availability Statement

The data that support the findings of this study are available in the supplementary material of this article.

[1] R. E. Blankenship, *Molecular Mechanisms of Photosynthesis*, 2nd ed., Wiley, Chichester, **2014**, p. 312.

[2] a) J. P. Dekker, R. Van Grondelle, *Photosynth. Res.* **2000**, *63*, 195–208; b) T. Cardona, A. Sedoud, N. Cox, A. W. Rutherford, *Biochim. Biophys. Acta Bioenerg.* **2012**, *1817*, 26–43.

[3] a) A. Zouni, H. T. Witt, J. Kern, P. Fromme, N. Krauss, W. Saenger, P. Orth, *Nature* **2001**, *409*, 739–743; b) B. Loll, J. Kern, W. Saenger, A. Zouni, J. Biesiadka, *Nature* **2005**, *438*, 1040–1044; c) K. N. Ferreira, T. M. Iverson, K. Maghlaoui, J.

Barber, S. Iwata, *Science* **2004**, *303*, 1831–1838; d) Y. Umena, K. Kawakami, J.-R. Shen, N. Kamiya, *Nature* **2011**, *473*, 55–60.

[4] a) R. Croce, H. van Amerongen, *Science* **2020**, *369*, eaay2058; b) T. Renger, E. Schlodder, *J. Photochem. Photobiol. B* **2011**, *104*, 126–141; c) A. Sirohiwal, F. Neese, D. A. Pantazis, *J. Am. Chem. Soc.* **2020**, *142*, 18174–18190.

[5] a) H. Miyashita, H. Ikemoto, N. Kurano, K. Adachi, M. Chihara, S. Miyachi, *Nature* **1996**, *383*, 402–402; b) D. J. Nürnberg, J. Morton, S. Santabarbara, A. Telfer, P. Joliot, L. A. Antonaru, A. V. Ruban, T. Cardona, E. Krausz, A. Boussac, A. Fantuzzi, A. W. Rutherford, *Science* **2018**, *360*, 1210–1213; c) F. Gan, S. Zhang, N. C. Rockwell, S. S. Martin, J. C. Lagarias, D. A. Bryant, *Science* **2014**, *345*, 1312; d) V. Mascoli, L. Bersanini, R. Croce, *Nat. Plants* **2020**, *6*, 1044–1053.

[6] a) H. Pettai, V. Oja, A. Freiberg, A. Laisk, *Biochim. Biophys. Acta Bioenerg.* **2005**, *1708*, 311–321; b) A. Thapper, F. Mamedov, F. Mokvist, L. Hammarström, S. Styring, *Plant Cell* **2009**, *21*, 2391–2401.

[7] N. L. Greenbaum, D. Mauzerall, *Biochim. Biophys. Acta Bioenerg.* **1991**, *1057*, 195–207.

[8] a) J. L. Hughes, P. Smith, R. Pace, E. Krausz, *Biochim. Biophys. Acta Bioenerg.* **2006**, *1757*, 841–851; b) F. Mokvist, J. Sjöholm, F. Mamedov, S. Styring, *Biochemistry* **2014**, *53*, 4228–4238.

[9] a) F. Mokvist, F. Mamedov, S. Styring, *J. Biol. Chem.* **2014**, *289*, 24630–24639; b) E. Schlodder, F. Lendzian, J. Meyer, M. Çetin, M. Brecht, T. Renger, N. V. Karapetyan, *J. Am. Chem. Soc.* **2014**, *136*, 3904–3918.

[10] A. Sirohiwal, F. Neese, D. A. Pantazis, *J. Chem. Theory Comput.* **2021**, *17*, 1858–1873.

[11] F. Müh, M. Plöckinger, T. Renger, *J. Phys. Chem. Lett.* **2017**, *8*, 850–858.

[12] a) H. Tamura, K. Saito, H. Ishikita, *Proc. Natl. Acad. Sci. USA* **2020**, *117*, 16373–16382; b) H. Tamura, K. Saito, H. Ishikita, *Chem. Sci.* **2021**, *12*, 8131–8140.

[13] A. R. Holzwarth, M. G. Müller, M. Reus, M. Nowaczyk, J. Sander, M. Rögner, *Proc. Natl. Acad. Sci. USA* **2006**, *103*, 6895–6900.

[14] a) K. Saito, T. Ishida, M. Sugiura, K. Kawakami, Y. Umena, N. Kamiya, J.-R. Shen, H. Ishikita, *J. Am. Chem. Soc.* **2011**, *133*, 14379–14388; b) D. Narzi, D. Bovi, P. De Gaetano, L. Guidoni, *J. Am. Chem. Soc.* **2016**, *138*, 257–264.

[15] a) B. A. Diner, E. Schlodder, P. J. Nixon, W. J. Coleman, F. Rappaport, J. Lavergne, W. F. J. Vermaas, D. A. Chisholm, *Biochemistry* **2001**, *40*, 9265–9281; b) M. L. Groot, N. P. Pawlowicz, L. J. G. W. van Wilderen, J. Breton, I. H. M. van Stokkum, R. van Grondelle, *Proc. Natl. Acad. Sci. USA* **2005**, *102*, 13087–13092; c) E. Romero, I. H. Van Stokkum, V. I. Novoderezhkin, J. P. Dekker, R. Van Grondelle, *Biochemistry* **2010**, *49*, 4300–4307; d) I. V. Shelaev, F. E. Gostev, M. I. Vishnev, A. Y. Shkuropatov, V. V. Ptushenko, M. D. Mamedov, O. M. Sarkisov, V. A. Nadtochenko, A. Y. Semenov, V. A. Shuvalov, *J. Photochem. Photobiol. B* **2011**, *104*, 44–50; e) H.-G. Duan, V. I. Prokhorenko, E. Wientjes, R. Croce, M. Thorwart, R. D. Miller, *Sci. Rep.* **2017**, *7*, 12347; f) A. Pavlou, J. Jacques, N. Ahmadova, F. Mamedov, S. Styring, *Sci. Rep.* **2018**, *8*, 2837.

[16] N. Ahmadova, F. Mamedov, *Photosynth. Res.* **2018**, *136*, 93–106.

[17] H. Pettai, V. Oja, A. Freiberg, A. Laisk, *FEBS Lett.* **2005**, *579*, 4017–4019.

[18] a) S. Zhen, M. W. van Iersel, *J. Plant Physiol.* **2017**, *209*, 115–122; b) S. Zhen, B. Bugbee, *Front. Plant Sci.* **2020**, *11*, 581156; c) S. Zhen, B. Bugbee, *Plant Cell Environ.* **2020**, *43*, 1259–1272.

[19] E. Wientjes, H. van Amerongen, R. Croce, *J. Phys. Chem. B* **2013**, *117*, 11200–11208.